Title

Mechanics of pulmonary airways: Linking structure to function through constitutive modeling, biochemistry, and histology

Authors

Eskandari, Mona
Nordgren, Tara M
O'Connell, Grace D

Publication Date

2019-10-01

DOI

10.1016/j.actbio.2019.07.020

Peer reviewed

Mechanics of Pulmonary Airways: Linking Form to Function Through Experimentally Informed Constitutive Models, Biochemical Analysis, and Histology

Mona Eskandari[a,b], Grace D. O'Connell[b]

[a]*Department of Mechanical Engineering, Department of Bioengineering, School of Medicine BREATHE Center, University of California at Riverside, Riverside CA, 92521*

[b]*Department of Mechanical Engineering, University of California at Berkeley, Berkeley CA, 94720*

Abstract

The unknown relationship between pulmonary structure and function is increasingly becoming the focus of lung mechanics research as it imposes significant limitations on medical advancements and clinical translation. Breathing is an interaction between fluid flow and structural motion, yet the lack of experimentally measured material properties disconnects air forces from tissue deformations. To address these needs, we characterize the mechanical properties of porcine airways based on uniaxial tensile experiments, accounting for anisotropy and heterogeneity. We formulate the first pulmonary constitutive model capturing proximal and distal bronchial region effects to determine airways' collagen fibers and extrafibrillar matrix role in a structurally-motivated mechanical function. The strain-energy function combines a matrix contribution, (selected from six common constitutive models: compressible NeoHookean, unconstrained Ogden, uncoupled Mooney-Rivlin, incompressible Ogden, incompressible Demiray and incompressible NeoHookean), reinforced with a fiber model, selected from an exponential or polynomial function. Agreement between the experimental data and model fit is determined by minimizing residual error, and maximizing R^2, considering uniqueness and sensitivity. The incompressible Demiray model describing the matrix term complemented by an exponential function for the fiber contribution was deemed most appropriate for all bronchial regions. Model stress-stretch behavior, resulting parameters and deviations, matrix versus fiber contributions, and parameter correlations to mechanical properties are compared across trachea, large bronchi, and small bronchi regions. Identified mechanical parameters and significant material heterogeneity motivates biochemical analysis and histology imaging to explore the impact of tissue composition and structural form. Correlations between mechanical function to collagen and glycosaminoglycan content requires further investigation, however microstructural observations suggest evolution of tissue architecture from proximal to distal airways, namely transformation of fiber curvature and crimp, may be responsible for regional functionality of bronchial tissue. Our systematic pulmonary tissue characterization provides experimentally informed, structurally-reinforced, mathematical models capturing bronchial material response lacking

in the literature, enabling fluid-structure interaction simulations, and ultimately aiming to advance disease diagnosis and progression through computational techniques.

Keywords:
Lung Mechanics; Biochemistry; Histology; Material Behavior; Constitutive Law; Tissue Characterization

1. Introduction

Billions of dollars are spent annually on the leading cause of death worldwide; unknown to people, lung disease is responsible for claiming millions of lives each year (2; 8; 76; 100). Current lung biomechanics research consists of predominantly single-mechanism approaches: the fluid mechanics community explores turbulent flow, particle deposition, and branching algorithms (49; 53; 66; 99; 102; 104), and the solid/structural mechanics community investigates trachea, alveolar, and parenchymal tissue response (23; 41; 61; 62; 72; 92); yet the lung is both a flow and structure system. The knowledge junction between the fluid-structure interaction of the lung remains disconnected because the scientific literature on airway material properties is scarce.

The absence of biomechanical experimental tissue characterization limits research insights. Modeling obstruction patterns caused by inflammation and constriction, or tissue remodeling caused by chronic endurance of lung diseases, such as asthma or bronchitis, rely heavily on the mechanical properties of the airways (43; 20; 21; 45; 56; 57; 71); these studies are constrained to use generic material properties spanning multiple orders of magnitude. Analogously, majority of fluid mechanics studies analyzing flow employ rigid airway geometry despite the lungs transporting liters worth of volume per breath (74); accounting for tissue deformation during breathing yields drastically altered particle deposition results (54; 94; 103). Physiologically relevant insights will continue to remain elusive because of undocumented bronchial mechanics. Current deficiencies, including significant oversimplification of lung biomechanics research (e.g. substitution of arterial constitutive laws in lieu of pulmonary behavior), can be overcome through relational exploration of coupled breathing stresses and deformation of isolated airway measures (16; 42; 48; 50; 61; 103).

The complexity of the bronchial network challenges the acquisition of mechanical properties, temporal responses, and morphological structures responsible for airway deformation and stress distribution (39; 98). The multi-layered composition of the airways consists of soft tissue attached to cartilaginous substructures, ring-like in proximal regions evolving into separate scales in distal bronchi (19). The soft connective tissue between sections of cartilage rings bears the bulk of deformation during breathing, while mechanics studies have characterized the more rigid cartilage (14; 33; 50; 88**?**). The distal bronchi are imbedded in spongy elastic parenchyma (69; 86). The structure complicates experimental design

Email address: eskandar@ucr.edu (Mona Eskandari)
URL: bmech.engr.ucr.edu (Mona Eskandari)

and procurement of a reproducible technique (24; 46; 78; 83; 92). These challenges restrict most studies to the investigation of the trachea, the most readily accessible airway (16; 33; 79; 82; 89; 91; 95; 97), whereas intraparenchymal airways form nearly the entirety of lung volume, and are more relevant sites of disease obstruction (10; 17; 93). Advancements in pulmonary research requires instituting complete mechanics based on experimental measures accounting for proximally and distally located airways.

To address these needs, we utilize extensive uniaxial tensile porcine bronchi experiments to obtain a novel airway-specific constitutive relation capturing the behavior of various bronchial regions and calibrated by orientation-informed fiber reinforcement. Trachea, large bronchi, and small bronchi samples are categorized by solely matrix engagement or combined matrix and fiber engagement depending on circumferential or axial testing orientation, respectively. Six common nonlinear hyperelastic compressible and incompressible models describe the matrix response (13; 35; 78; 82); the best fit to experimentally acquired preconditioned stress-strain data is then complemented by either an exponential or polynomial fiber model option (89; 37). All parameter fits are presented and the best overall matrix plus fiber strain-energy function for all bronchial regions is found. The resulting constitutive parameters are compared across region to decipher mechanical function variation. Tissue stiffness is correlated to mechanical parameters to establish possible correlations. The proportional matrix-fiber contribution to the stress-strain response is compared for the trachea, large bronchi, and small bronchi, and the model's sensitivity to experimental variation in material parameters is explored. The significant differences in parameter fits suggest mechanical heterogeneity and potential variation in tissue composition between the trachea, large bronchi, and small bronchi, which is further explored through biochemical analysis of glycosaminoglycan (GAG) and collagen content. Qualitative histological observations reveal mucosa microstructure most readily changes with respect to region and suggest tissue architecture and form may be extremely influential in dictating the material property variations of the proximal and distal airways.

The findings of this study address a glaring void in lung biomechanics research, a necessary prerequisite to clinical translation. The results yield critical information to construct physiologically relevant computational models capable of reproducing the anisotropic and heterogenous response of the bronchial tree. This work facilitates extension to human tissue with expected similarities (65; 59), and to diseased states with suspected altered mechanical properties (12; 34; 42; 47; 56). Establishing the biomaterial properties of bronchial tissue is central to lung research progress; we provide the foundation for understanding airway biomechanics, facilitating the creation of disease diagnostics, surgical planning, and predictive technologies, aimed at advancing pulmonary medicine.

2. Materials and Methods

The complexity of lung tissue requires extensive experimental protocol development and design iteration, as stated previously. We briefly describe specimen handling and dissection here, directing the reader to prior investigating for detailed tissue methodologies (24). Here we focus on the development of an pulmonary constitutive model representative of the me-

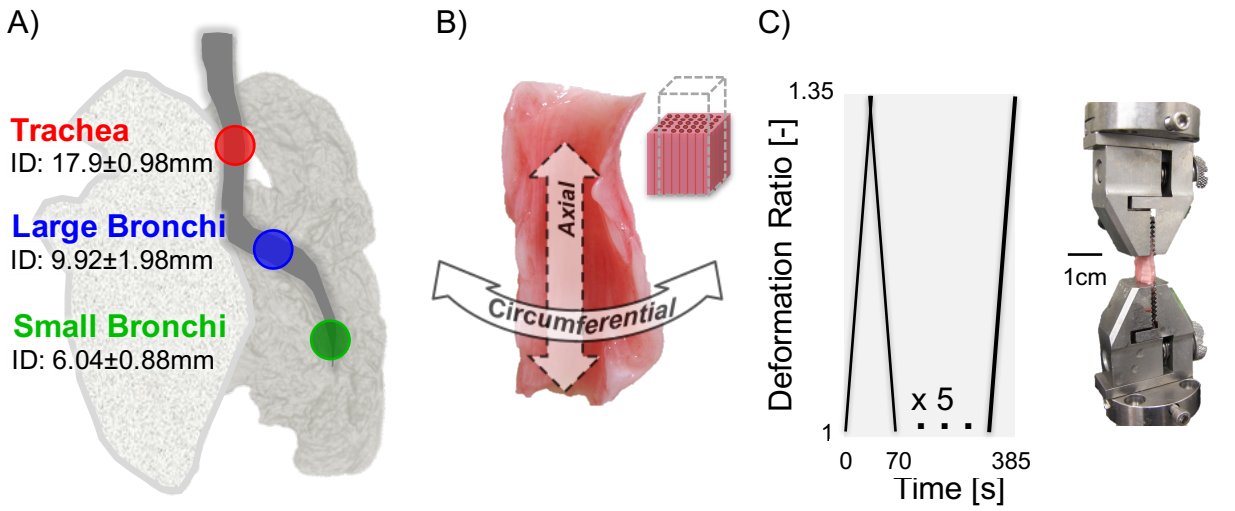

Figure 1: Illustration of experimental protocol dissecting samples from porcine lung. (A) Three regions of extra- and intraparenchymal sample procurement denoted as the trachea, large bronchi, and small bronchi. (B) For each of these regions, samples were loaded in two orientations, circumferential and axial, with fibers aligned longitudinally. (C) Six categorical samples were each subjected to preconditioning protocol, elongating the tissue to a ratio of 1.35 five times before using the stress-strain response from the sixth loading curve to inform constitutive relationships.

chanical response of varying regions of the bronchial tree, highlighting and further exploring the relationship between pulmonary structure and function from tissue composition and image observations.

2.1. Lung Specimens

Uniaxial tensile tests were performed on samples collected from the trachea, large bronchi, and small bronchi regions of five porcine specimens with n>30 viable measurements per animal specimen (totaling more than 150 viable samples). Samples were evenly distributed amongst porcine hosts and categorical orientation and region to avoid statistical skew. Figure 1 illustrates specificied regions with categorical inner diameter (ID) measurements, and airway wall tissue specimens, with soft tissue composed of the mucosa and submucosa, oriented based on circumferential and axial directions with illustrated fiber alignment (63). These six tissue sample categories measured 3-4mm wide, 8-9mm long, and 1-2mm thick and were subjected to a deformation ratio of 1.35, preconditioned five times with the sixth loading stress-strain response analyzed. Samples were stretched at a deformation ratio rate of 0.01/sec (24; 89).

2.2. Modeling and Data Analysis

The established anisotropy of the tissue(24) motivated use of structurally-reinforced strain-energy function to explore regional behavior. Inspection of tissue morphology informed fiber orientation and was confirmed by microscopy observations in previous airway

studies and histology performed in this work (11; 55). Equations 1 and 2 employed the structural reinforcement differentiation between circumferential and axial samples to formulate the compound the strain-energy function: circumferential samples assumed engagement of solely the extracellular matrix while axially tested samples engaged collagen and elastic fibers in addition to the matrix (36; 37; 40; 81; 87).

$$\psi_{circumferential} = \psi_{matrix} \tag{1}$$

$$\psi_{axial} = \psi_{matrix} + \psi_{fiber} \tag{2}$$

The experimental data fitting was performed in two sequential parts. First the matrix portion of the strain-energy function informed by circumferentially tested samples was established, as it reappears for the axial tissue description. Six models, three compressible (compressible NeoHookean, unconstrained Ogden, and uncoupled Mooney-Rivlin) and three incompressible (incompressible Ogden, incompressible Demiray and and incompressible Neo-Hookean) were considered. The best fit matrix model designated from circumferential samples is used to fit axially tested samples. Axially samples had a fiber term in addition to a matrix term (equation 2) with the fiber term selected as either a two-term exponential or polynomial expression. The parameters for the circumferential term of the axial samples is not fixed according circumferential samples, rather bounded by the circumferentially-informed samples' averages ± standard deviation. Thus, the best fit fiber-reinforced constitutive model representing all three regions (trachea, large bronchi, and small bronchi) was designated. Parameter fits differed between region and significance was explored. Axial samples were used to find proportional stress contributions: the matrix stress portion from the derivative of ψ_{matrix} normalized by the total stress value denoted the matrix stress contribution (67). Similarly, fiber stress contribution was found from ψ_{fiber}. While both axial and circumferential samples of the three regions had resulting matrix term parameters, the values did not differ significantly and reflected same regional trends. This was expected and the approach was used as a mathematical check.

2.2.1. Uniaxial Tensile Testing Continuum Mechanics

Nonlinear equations of continuum mechanics were used to mathematically describe tissue deformation. The deformation map $\phi(X)$, which relates the undeformed to deformed state is used to define the deformation gradient $F(X)=\nabla\phi(X)$, which is a diagonal matrix of form (35).

$$F = \begin{bmatrix} \lambda_1 & 0 & 0 \\ 0 & \lambda_2 & 0 \\ 0 & 0 & \lambda_3 \end{bmatrix} \tag{3}$$

λ_1, λ_2 and λ_3 are the principle stretches of the tissue and λ_3 is aligned with the device grips elongation direction (Instron 5848 Microtester and 10N load cell). λ_3 is described as $\lambda_3 = 1 + d/H$, where d is the grip displacement normalize by the tissue sample height H. We assume λ_1 and λ_2 contract equally in relation to Poisson's ratio, a free parameter for compressible NeoHookean, unconstrained Ogden, and uncoupled Mooney-Rivlin models.

Generally F becomes

$$F = \begin{bmatrix} \lambda_3^{-\nu} & 0 & 0 \\ 0 & \lambda_3^{-\nu} & 0 \\ 0 & 0 & \lambda_3 \end{bmatrix} \tag{4}$$

for large deformation Poisson's effect. F further reduces to $F = diag(\sqrt{\lambda_3}; \sqrt{\lambda_3}; \lambda_3)$ for incompressible NeoHookean, incompressible Ogden, and incompressible Demiray models where $\nu = 0.5$ (36).

2.2.2. Constitutive Relations

We use six phenomenological hyperelastic constitutive relations to describe the matrix strain-energy contribution and subsequently augment the result with two fiber strain-energy functions to account for anisotropy through structural reinforcement. Viscous and porous effects are ignored, however, unlike majority of biological studies we did not assume compressibility *a priori* and allowing for compressibility to be explored through model performance (13; 55). Preliminary digital image correlation studies substantiated our assumption of homogenous tissue deformation. The strain-energy functions commonly found in the literature are expressed in terms of material parameters and invariants, the latter can be related to the principle stretch λ_3. Here we have expressed the common form and included the complete derivation methodology for compressible Neo-Hookean for clarity (22). The same approach is followed for all remaining constitutive model derivations.

For compressible NeoHookean (C-NH):

$$\psi_{C-NH}(I_1(\lambda_3), J(\lambda_3)) = \frac{1}{2}\,\mu\,[I_1 - 3\,] + \frac{\lambda}{2} ln(J)^2 - \mu ln(J) \tag{5}$$

μ and λ act as Lamé constants, (λ not to be confused with experimental stretch λ_3). I_1 and J are the first invariant and Jacobian respectively, and are related to λ_3 and include ν in their formulations. Therefore, the compressible NeoHookean model has three parameters ν, μ, and λ with units [-], [kPa], and [MPa].

P is first Piola-Kirchhoff stress and the derivative of the strain-energy function with respect to F. P is found using the chain and product rules:

$$P = \frac{\delta \psi_{C-NH}}{\delta F} = \frac{\delta \psi_{C-NH}}{\delta I_1} \frac{\delta I_1}{\delta \lambda_3} \frac{\lambda_3}{\delta F} + \frac{\delta \psi_{C-NH}}{\delta J} \frac{\delta J}{\delta \lambda_3} \frac{\lambda_3}{\delta F}. \tag{6}$$

P is a tensor but we are only interested in P_{33} resulting from the stretch in the 33 direction. P_{33} was directly measured from tensile testing (55), where $P_{33} = f_z/(WT)$ and f_z is the measured force from the load cell, W is the tissue width and T is the tissue thickness. The product of W and T provides the sample cross-sectional area in the reference configuration.

The first invariant is $I_1 = trace(C)$ where C is the right Cauchy-Green deformation tensor $C = F^t F$, and F is a function of λ_3 based on compressible or incompressible models; for compressible NeoHookean F is $F = diag(\sqrt{\lambda_3}; \sqrt{\lambda_3}; \lambda_3)$. Therefore, in terms of λ_3, $I_1 = 2\lambda_3^{-2\nu} + {\lambda_3}^2$. The Jacobian J is defined as $J = det(F) = \lambda_3^{1-2\nu}$ (1). The partial

derivatives are (87):

$\frac{\delta\psi_{C-NH}}{\delta I_1} = \frac{\mu}{2}$;

$\frac{\delta I_1}{\delta\lambda_3} = -4\nu\lambda_3^{(-2\nu-1)} + 2\lambda_3$;

$\frac{\delta\psi_{C-NH}}{\delta J} = \frac{\mu}{J} + \frac{\lambda}{J}ln(J)$;

$\frac{\delta J}{\delta\lambda_3} = (1-2\nu)\lambda_3^{-2\nu}$;

and trivially, $\frac{\lambda_3}{\delta F_{33}} = 1$.

F_{33} denotes the third diagonal of F which will extract the corresponding P_{33} of P. Evaluating $\lambda_3 = 1$ in equation 6 results in $P_{33} = 0$, as expected. For simplicity we will call $P_{33} = P$ from here on.

The remaining five models' stress expressions are similarly derived from their strain-energy expressions.

Unconstrained Ogden (U-O), 4 parameters:

$$\psi_{U-O}(\lambda_3, J(\lambda_3)) = \frac{1}{2}c_p(J-1)^2 + \frac{c_1}{\alpha^2}(\lambda_1^\alpha + \lambda_2^\alpha + \lambda_3^\alpha - \alpha ln(J)), \tag{7}$$

where c_1 [kPa] is a coefficient, α [-] is an exponent, c_p [MPa] acts as a bulk-like modulus, and ν is encapsulated within F and is Poisson's ratio [-]. Recall λ_1 and λ_2 are related to λ_3 through F where $\lambda_1 = \lambda_2 = \lambda_3^{-\nu}$.

Uncoupled Mooney-Rivlin (U-MR), 4 parameters:

$$\psi_{U-MR}(I_1(\lambda_3), I_2(\lambda_3)J(\lambda_3)) = c_1(I_1-3) + c_2(I_2-3) - 2(c_1+2c_2)ln(J) + \frac{\lambda}{2}ln(J)^2 \tag{8}$$

where I_2 is the second invariant expressed as $I_2 = \frac{1}{2}[(trace(C))^2 + trace(C^2)] = {\lambda_3}^{-4\nu} + 2{\lambda_3}^{(2-2\nu)}$, and c_1 and c_2 are parameters [MPa].

Incompressible Ogden (I-O), 2 parameters:

$$\psi_{I-O}(\lambda_1(\lambda_3), \lambda_2(\lambda_3)) = \frac{2\mu}{\alpha^2}\left(\lambda_1^\alpha + \lambda_2^\alpha + \lambda_3^\alpha - 3\right) \tag{9}$$

where μ [kPa] is a coefficient, α [-] is an exponent, and λ_1 and λ_2 are previously described.

Incompressible Demiray (I-D), 2 parameters:

$$\psi_{I-D}(I_1(\lambda_3)) = \frac{\mu}{2\beta}\left(exp[\beta(I_1 - 3] - 1\right) \tag{10}$$

where μ [kPa] is a coefficient, β [-] is an exponent , and I_1 is previously described.

Incompressible NeoHookean (I-NH), 1 parameter:

$$\psi_{I-NH}(I_1(\lambda_3)) = \frac{\mu}{2}(I_1 - 3) \tag{11}$$

where μ [kPa] is a coefficient.

ψ_{fiber} for the axial samples consisting of a fiber portion is selected from two-term exponential or polynomial expressions for the strain-energy expression, and derived as the matrix models were described earlier. The resulting fiber expression is summed with the matrix expression as in equation 2, and the stress is ψ_{axial}'s derivative.

Fiber Exponential expression, 2 parameters:

$$\psi_{exp} = \frac{k_1}{k_2}(exp^{[k_2(I_4-1)^2]} - 1) \tag{12}$$

where I_4 is the fourth invariant, dependent on the fiber direction, for which we have aligned with the force; therefore, I_4 simplifies to $I_4 = {\lambda_3}^2$ (81; 5). k_1 [kPa] acts as a coefficient and k_2 [-] as an exponent.

Fiber Polynomial expression, 2 parameters (15):

$$\psi_{poly} = k_1(I_4 - 1)^2 + k_2(I_4 - 1)^3 \tag{13}$$

where I_4 is used again and reduces to $I_4 = {\lambda_3}^2$ (37). k_1 and k_2 both act as coefficients [kPa].

2.3. Material Model Calibration

MATLAB's non-linear least squares algorithm, *lsqnonlin*, was used to minimize the difference between the model generated first Piola-Kirchhoff stress P and experimentally measured stress P^{exp}. All experimentally gathered data was mathematically interpolated onto 1001 equally spread points to avoid sample measuring bias. All constitutive model parameters were free to range between $[-\infty, +\infty]$, except for ν which was constrained to range between [0, 0.5], and the uncoupled Mooney-Rivlin parameter c_2, which was negative for concavity $[-\infty, 0]$ (35). The initial guesses of each parameter was multiplied by a random coefficient and run several times to compare solution integrity. Initial guesses were also varied by two orders of magnitude and subject to multiple runs. Uniqueness was a criteria for model fitting and non-unique models were identified. A Bland Altman analysis was used to provide a measure of agreement between the model and experimental data. The coefficient of determination $R^2 = 1 - S^{residual}/S^{total}$ was used to determine goodness of fit, where the sum of residual squares is $S^{residual}{=}\Sigma_i^{1001}(P_i^{exp} - P_i)^2$, P_i^{exp} and P_i are experimental and model values, respectively. The total sum of squares is $S^{total}{=}\Sigma_i^{1001}(P_i^{exp} - P_{mean})^2$, and P_{mean} is the mean of the observed data (13). The mean of the residual error $\Sigma_i^{1001}(P_i^{exp} - P_i)$ was used in conjunction with R^2. The best model was defined as one which had both R^2 nearest to unity and smallest residual error.

2.4. Model Sensitivity

A sensitivity analysis was conducted to inform how the parameter calibrations' deviations impact the stress-stretch response of the resulting best fit model (32; 68). For the circumferential samples fitted to the incompressible Demiray model, one parameter, either μ or β, was fixed at its average regional value while the other parameter was varied from its average by its standard deviation. Similarly, for the axial samples, either μ, β, k_1 or k_2 were varied at ±standard deviation while the other three parameters were fixed at their average response. Analysis showed how parameter calibration to experimental tensile behavior affects specific parameters' impact on the stress-strain response, further distinguished by region.

2.5. Biochemistry

One porcine lung was used to quantify biochemical composition for the trachea, large bronchi, and small bronchi. A 4mm diameter biopsy punch was used to prepare three specimen samples from each region, dissecting only the soft tissue removed from the cartilage layer. The wet weight of freshly prepared specimens was acquired and specimens were dried overnight in lyophilizer. After drying, dry weights were acquired to calculate the water content as the difference between wet and dry weights normalized by the wet weight. After freeze-drying, the remaining precipitate was re-suspended in 1 mL of 0.5 mg/mL proteinase K (PK digest) and digested overnight at 56C. DNA content was determined using the PicoGreen Kit (Invitrogen). The glycosaminoglycan (GAG) content was determined using 1,9-dimethylmethylene blue (DMMB). A 100μl aliquot of PK digested sample was prepared for the hydroxyproline assay through acid hydrolysis (12M HCl). The ratio of hydroxyproline to collagen was assumed to be 10.0. GAG and collagen contents were normalized by wet weight, dry weight and DNA content. ()[*Grace References?].

2.6. Histology

Representative sample specimens for each region (trachea: 19.22mm ID, large bronchi: 11.8mm ID, small bronchi: 6.22mm ID) were cut from the airway using a scalpel and fixed in 4% formaldehyde solution (71). Gladstone Institutes Histology and Light Microscopy Core provided histology services for Masson's Trichrome and Hematoxylin and Eosin staining (11; 78). Dehydrated samples were embedded in paraffin wax blocks and sliced 2-10μm thick. Red and pink colors highlighted cytoplasm, keratin, muscle, and intercellular fiber (elastin); black stained cell nuclei; and blue stained collagen and mucus (25). Slides were imaged with an digital camera (AmScope FMA037, Irvine CA) attached to an upright microscope (Olympus CKX31).

2.7. Statistics and Correlations

After finding the best model, only 1-2 sample points per region were identified as outliers exceeding 1.5 times the interquartile range (Q1-Q3), and were omitted. All values were subject to a Box-Cox transformation, followed by a one-way analysis of variance (ANOVA) and Bonferroni multiple comparison adjusting for groups. Calculations were done in MATLAB's Statistics Toolbox, with p-values less than 0.05 denoting significance. Resulting

constitutive model parameter calibrations, experimental biochemistry values and correlations were analyzed. Spearman's correlation analysis was used to find inter-relationships between constitutive parameters and correlate to experimental measures (24). Correlations between constitutive parameters and the pseudoelastic stiffness modulus E were deemed significant (32; 68). All correlations are reported and significant p-values with strong correlations (ρ>0.7) were graphed and analyzed (correlations defined as strong: ρ>0.7, moderate: 0.7>ρ>0.5, weak: ρ<0.5) [8].

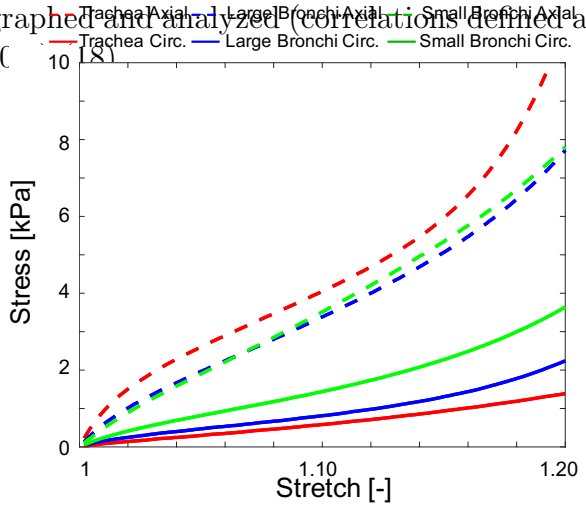

Figure 2: Average curves of each categorical sample orientation and region. Axial samples portray greater stress response and non-linearity than circumferential samples for given strain range. Circumferential small bronchi exhibits greater stress ranges and pseudoelastic stiffness modulus (slope) than trachea and large bronchi counterparts (24).

3. Results

3.1. Stress-Stretch Response

The average categorical sample response grouped by orientation (axial and circumferential) and region (trachea, large bronchi, and small bronchi) is shown in Figure 2. The linear slope of the stress-strain response in the small stretch region (<1.15) is called the psuedoelastic modulus E and acts as a measure of material stiffness (24). For trachea, large bronchi, and small bronchi axially oriented samples, E is greater compared to circumferential counterparts. Notably, small bronchi circumferential samples have a greater stiffness than either circumferential trachea or large bronchi. The distinct material anisotropy as seen in Figure 2 was accounted for in the formulation of constitutive models through two-part complementary matrix and fiber strain-energy function. The heterogenous response was considered by analyzing each region separately.

3.2. Constitutive Model Performance

The performance of each model fit (colored lines) to a representative experimental sample (dotted line) is shown in Figure 3. Fits were categorized by tissue testing orientation; some models performed better for specific regions but their overall performance for all regions were

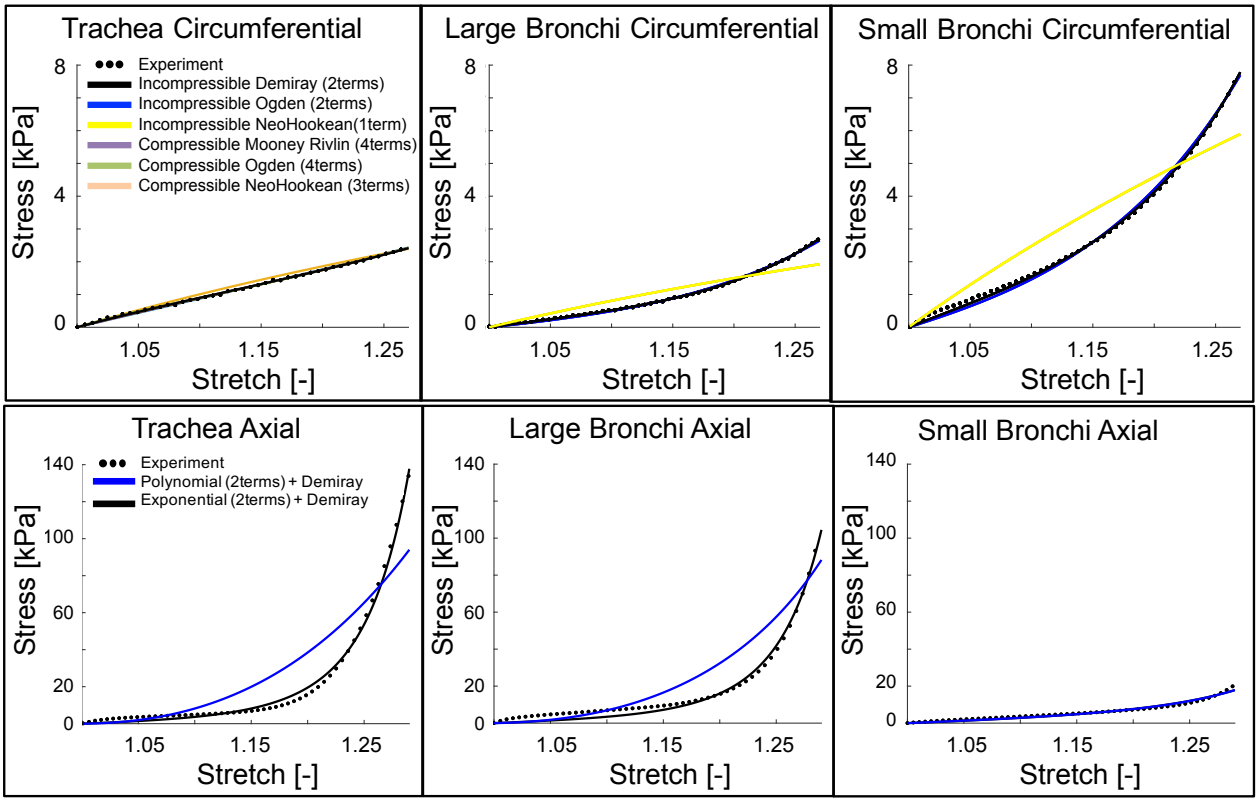

Figure 3: Representative circumferential and axial sample data fitted to various constitutive models. Circumferential tissue engaged the tissue matrix while axial tissue engaged both fiber and matrix components; circumferential samples were fit to homogenous compressible and incompressible models, with incompressible Demiray providing the best fit (top row, black line). Axial tissues were subsequently fit to fiber-reinforced combined constitutive law, adopting incompressible Demiray for the matrix contribution and exponential term for the fiber response (bottom row, black line).

averaged and evaluated. The best fit matrix model (deemed best based on multiple fitting metrics) to circumferential data was found to be the incompressible Demiray function. Five of the six models had R^2 >0.95, and incompressible NeoHookean had R^2=0.816, understandably so, since it fit a single term only. Since incompressibility was not assumed beforehand, compressible models were analyzed but found to be inaccurate compared to better performing incompressible models: compressible Neohookean had visibly poor fits despite R^2= 0.964; unconstrained Ogden and uncoupled Mooney-Rivlin had non-unique fits, with more parameters than necessary. The incompressible models performed better overall. Incompressible Demiray was the best matrix model (R^2=0.997, residual=-0.041MPa), followed by its 2-term counterpart, Incompressible Ogden (R^2=0.995, residual=-0.088MPa), and having the smallest residual error. Adjusted R^2 was also considered to account for comparing varying number of parameters for fits, but the results of constitutive model performance were negligibly altered (R^2 changed by 10^{-5}.

With incompressible Demiray being the model function of choice for the matrix term, axial samples were fit by adding a fiber part to the strain-energy function to evaluate the performance of a 2-term exponential versus a polynomial expression. Both residual errors and R^2 values were better for an exponential term (R^2=0.991, residual=-0.175MPa). All

Matrix Response (Circumferential Samples)

Compressible Models

Neohookean	*Trachea*	*Large Bronchi*	*Small Bronchi*
ν [-]	0.483 ± 0.066	0.483 ± 0.066	0.484 ± 0.062
μ [kPa]	23.7 ± 39.32	147.2 ± 297.7	114.7 ± 166.1
λ [MPa]	-1119 ± 1113	-3759 ± 4920	-3252 ± 3335
Residual [MPa]=	*-0.131*		
R^2=	*0.964*		

Unconstrained Ogden			
ν [-]	0.336 ± 0.088	0.249 ± 0.139	0.236 ± 0.123
cp [Mpa]	39.50 ± 245.4	11.17 ± 49.75	8.862 ± 43.97
c1 [kPa]	127.1 ± 842.2	-287.2 ± 932.0	-321.8 ± 408.6
α [-]	-8.678 ± 36.29	2.046 ± 4.117	0.358 ± 7.558
Residual [MPa]=	*-0.125*		
R^2=	*0.963*		

Uncoupled Mooney-Rivlin			
ν [-]	0.425 ± 0.065	0.438 ± 0.086	0.436 ± 0.090
c1 [Mpa]	23.91 ± 66.68	452.2 ± 1822	964.8 ± 3996
c2 [Mpa]	-17.34 ± 90.11	-623.0 ± 3115	-1557 ± 6944
λ [MPa]	-498.9 ± 998.0	-2667 ± 5306	-1909 ± 2979
Residual [MPa]=	*-0.125*		
R^2=	*0.963*		

Incompressible Models

Ogden	*Trachea*	*Large Bronchi*	*Small Bronchi*
μ [kPa]	3.802 ± 2.128	2.584 ± 1.795	5.447 ± 4.555
α [-]	7.637 ± 3.603	13.80 ± 9.336	11.95 ± 5.575
Residual [MPa]=	-0.088		
R^2=	0.995		

Demiray			
μ [kPa]	2.215 ± 1.042	2.019 ± 1.331	3.764 ± 2.953
β [-]	2.508 ± 1.826	6.190 ± 4.211	5.171 ± 2.887
Residual [MPa]=	-0.041		
R^2=	0.997		

Incompressible Neohookean			
μ [kPa]	3.555 ± 2.540	9.354 ± 15.01	10.07 ± 11.09
Residual [MPa]=	0.387		
R^2=	0.819		

Fiber + Matrix Response (Axial Samples)

Exponential + Demiray	*Trachea*	*Large Bronchi*	*Small Bronchi*
k1 [kPa]	2.608 ± 2.687	1.937 ± 1.218	1.720 ± 1.257
k2 [-]	3.417 ± 2.79	2.007 ± 2.345	0.897 ± 1.850
μ [kPa]	2.682 ± 0.907	2.514 ± 1.146	5.063 ± 2.441
β [-]	1.204 ± 1.263	3.741 ± 3.124	2.650 ± 1.220
Residual [MPa]=	-0.175		
R^2=	0.991		

Polynomial + Demiray	*Trachea*	*Large Bronchi*	*Small Bronchi*
k1 [kPa]	2.068 ± 2.827	3.292 ± 3.051	3.763 ± 2.871
k2 [kPa]	11.49 ± 18.40	2.264 ± 5.000	0.651 ± 1.863
μ [kPa]	2.351 ± 1.008	2.645 ± 1.112	4.178 ± 2.514
β [-]	3.494 ± 1.429	7.123 ± 3.884	3.727 ± 2.361
Residual [MPa]=	0.607		
R^2=	0.959		

Table 1: Parameter fit values to matrix and fiber-reinforced matrix models. Circumferential samples were fit first to matrix model and the average parameter response bounded by the standard deviation was used to subsequently fit the matrix term of axial samples. Matrix models consist of both compressible models (compressible Neohookean, Unconstrained Ogden, Uncoupled Mooney-Rivlin) and incompressible models (Ogden, Demiray, incompressible Neohookean) to avoid premature assumption of material response. Fiber reinforced models utilized the best matrix model complemented with either exponential or polynomial functions. All models were evaluated based on uniqueness, sensitivity, and reproducibility, and agreement between model fit and experimental data was based on highest R^2 coefficient and lowest residual error.

models' residuals, R^2, and parameter average values and standard deviations are listed in Table 1.

3.3. Region-dependent Mechanical Behavior

The best strain-energy function composed of a matrix term informed by incompressible Demiray and fiber term informed by exponential expression resulted in 4 constitutive model parameters: μ, β, k_1, and k_2. Parameter averages and standard error of the mean are shown in Figure 4. The two terms μ and β corresponding to matrix response are informed by both circumferential (solid bars) and axial data (lined bars). k_1, and k_2 correspond to the fiber part of the strain-energy function, which is active for only axial data. Significant differences between the mechanical behaviors based on region are noted by $*$ with $p<0.05$. For μ and β the same relative regional trends between circumferential data and axial data are observed, however the absolute values change. There were significantly different μ and β between all regions and orientations, except no significant difference was noted between large and small circumferential β bronchi samples (difference was found between large and small axial bronchi however). k_1 had significantly different fits for all three regions but k_2 found small bronchi to differ with the trachea and large bronchi only. Difference of trachea

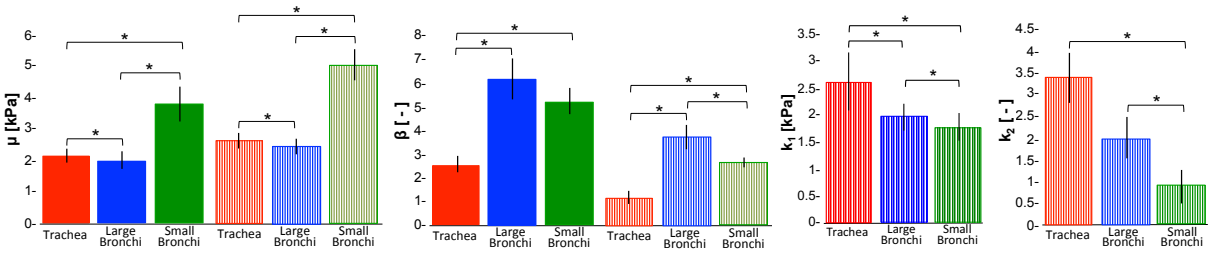

Figure 4: Average ± standard error of means of mechanical parameters values μ, β, k_1 and k_2 for incompressible Demiray model fit to circumferential samples (solid bars) and for fiber-reinforced combined constitutive model, incompressible Demiray and exponential, for axial samples (lined bars). μ and β are values for both circumferential and axial samples, since they result from the matrix expression and produce similar significant differences in fits to trachea, large bronchi, and small bronchi samples. k_1 and k_2 are parameters from the fiber-reinforced model informed by axial tissues, with fiber response. Regional differences in parameter fits are significant (*p<0.05).

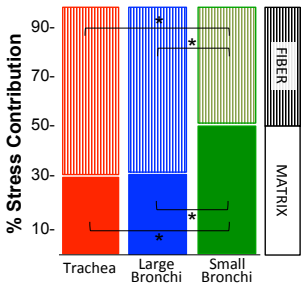

Figure 5: Percent stress contribution from the constitutive models' fiber or matrix term. For axial samples containing both matrix and fiber expressions, the proportion of the stress experienced by the tissues' matrix was less than the proportion of the stress experienced by the tissues' fiber, except for the small bronchi where it was a nearly even split. The small bronchi had significantly different division of stress hosted by the matrix versus the fiber, with the matrix having higher stress proportion. Conversely, the trachea's fibers had greater stress contribution than matrix, similar to the large bronchi (*p<0.05 significant).

and small bronchi mechanics is significant across all parameters. k_1 and k_2 values were found to continuously decrease from the trachea to small bronchi region. Surprisingly, the parameters did not generally increase or decrease between regions for matrix response μ and β. The large bronchi had significantly higher values for β. μ was the greatest amongst small bronchi, while small bronchi also had the smallest k_1 and k_2.

3.4. Matrix-Fiber Contribution to Function

Figure 5 illustrates the proportion of the tissue stress in tension carried by either the matrix (solid bars) or fiber (lined bars) relative to the total stress in the sample averaged over the whole stretch domain and for all samples grouped by region. The contribution compared by region found the matrix stress contribution is significantly lower for the trachea and large bronchi regions (29.2±19.2% and 32.0±15.7%) compared to the small bronchi (50.4±27.5%). The trachea and large bronchi's stress is mostly carried by the fiber portion of the strain-energy term (70.8±19.2% and (68.0±15.7%). Conversely, the small bronchi region splits the stress distribution nearly equally between the fiber and matrix formulations (50.4 and 49.6 ±27.5%). The difference between the mechanics defined by small bronchi's fiber versus matrix portion compared to both the trachea and large bronchi is significant.

	Correlation Coefficient ρ	p-value
Circumferential Tissue - Incompressible Demiray		
Interparameter Correlation		
β, μ	0.008	0.943
Correlation to Pseudoelastic Modulus		
E, β	0.255	**0.019**
E, μ	**0.907**	**0**

Axial Tissue - Incompressible Demiray + Exponential Fiber		
Interparameter Correlation		
β, μ	0.015	0.889
μ, k1	-0.064	0.558
μ, k2	-0.156	0.149
β, k1	0.112	0.303
β, k2	-0.252	**0.019**
k1, k2	-0.062	0.569
Correlation to Pseudoelastic Modulus		
E, μ	0.425	**0**
E, β	0.070	0.517
E, k1	**0.789**	**0**
E, k2	-0.073	0.504

Table 2: Correlation coefficients and significance from Spearman's method was used to find constitutive parameter relationships with mechanical properties and possible is interparameter correlation. Amongst circumferential and axial samples, no statistically significant strong or moderate interparameter correlation coefficient was found; β and k_2 had significant correlation but weak correlation coefficient (ρ=-0.252) (18). E was found to have significant correlations with mechanical parameters: amongst circumferential samples both μ and β had significant relationships to the modulus but only μ had a strong correlation coefficient (ρ=0.907). Similarly for axial samples, μ and k_1 were significantly correlated with E, but only k_1 had a strong correlation coefficient (ρ=0.789).

3.5. Correlations to Material Properties

μ and k_1 are coefficients in the matrix and fiber strain-energy calibrations while β and k_2 act as exponents. Inter-relationships between each constitutive parameter was explored by using a Spearman's correlation analysis, setting $p<0.05$ as significant and correlation coefficients $\rho>0.7$ as strong relationships indicative of correlations (strong: $\rho>0.7$, moderate: $0.7>\rho>0.5$, weak: $\rho<0.5$) (18). Table 2 lists both correlation coefficients and p-values for circumferential and axial data. Amongst experimental measures, the pseudoelastic stiffness modulus E was found to correlate with constitutive parameters. Interparameter correlations were ignored (only a weak correlation, ρ=-0.252, was found between β and k_2, p=0.019, and no other inter-parameter correlations were significant). Amongst circumferential data E was weakly correlated to β (ρ=0.255, p=0.019) and rather strongly correlated to μ (ρ=0.907, p=0). While the significant correlation to μ also existed for axial samples (p=0), the correlation weakened (ρ=0.425); k_1 was found to have significant and strong correlation to the material stiffness (ρ=0.789, p=0).

Figure 6 represents the relationship between the pseudoelastic modulus and μ for the circumferential data, and k_1 for the axial data. A linear relationship is fit to the data and equation provided. At the onset of tissue elongation (λ_3), the strain-energy expression simplifies to where the matrix stiffness is represented by μ and the fiber stiffness represented by k_1. This mathematical link can be observed in the direct positive relationship to E for both parameters. The slope of E-μ is also nearly half that of E-k_1.

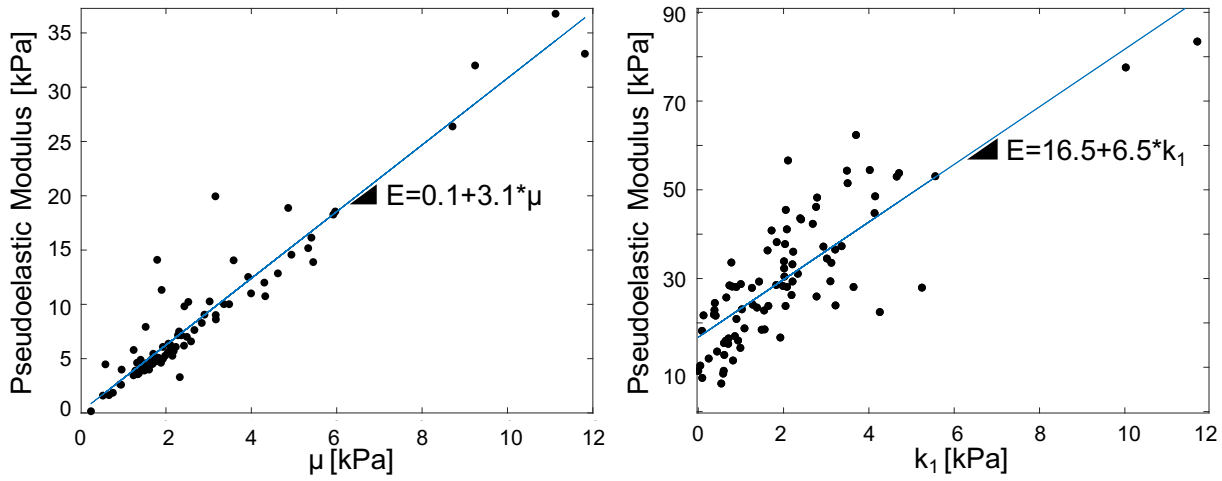

Figure 6: Correlations of pseudoelastic modulus values with circumferential samples' μ parameter (all regions) and axial samples' k_1 parameter (all regions). μ correlates with E with a strong coefficient correlation of 0.907, and k_1 correlates with E, also with a strong coefficient correlation of 0.789. While μ for axial samples is still significant (p=0), the correlation coefficient is weak. See Table 2 for correlation coefficients and p-values. Slope of linearly fit line to E versus circumferential μ or E versus axial k_1 are shown. The pseudoelastic modulus is a greater multiple of the mechanical fiber parameter k_1 than μ.

3.6. Model Behavior and Sensitivity Analysis

The model stress-stretch behaviors based on parameter calibrations are plotted in Figure 7 categorized by tissue orientation and region (parameter values listed in Table 1). For circumferential tissues the stress-stretch slope generally increases from the trachea to large bronchi and small bronchi. Circumferential tissues have smaller stress range than axial counterparts. This mirrors the trend discussed from Figure 2. Axial tissues show a declining stress-stretch slope from proximal to distal airways.

A sensitivity analysis was done to explore the variation in parameter fits to experimental stress-strain behavior and the impact on model performance. Greater sensitivity was defined as a widened range of stress-strain response due to parameter deviation in experimental data fitting. Deviation from the average model parameter response generally increased for increasing material stretch. Colored lines in Figure 7 illustrate the impact of each parameter's standard deviation on the model behavior. Circumferential samples showed μ and β extended the stress-strain range in small bronchi regions the most. The model was more sensitive to μ than β for all three regions. Axial samples' fiber parameters k_1 and k_2 exhibit greater sensitivity than matrix counterparts μ and β. For axial samples, μ and β are most sensitive for small bronchi compared to trachea and large bronchi. Conversely, k_1 and k_2 exhibit the widest range of stress-stretch response for the trachea. k_1 causes the most expansive stress-strain range amongst all axial responses.

3.7. Tissue Composition

Glycosaminoglycans (GAG) content is shown as a percentage of dry weight per trachea, large bronchi and small bronchi region in Figure 8. DNA content mirrored GAG trends (not shown). Small bronchi GAG content (2.47±0.04%) was significantly greater than large

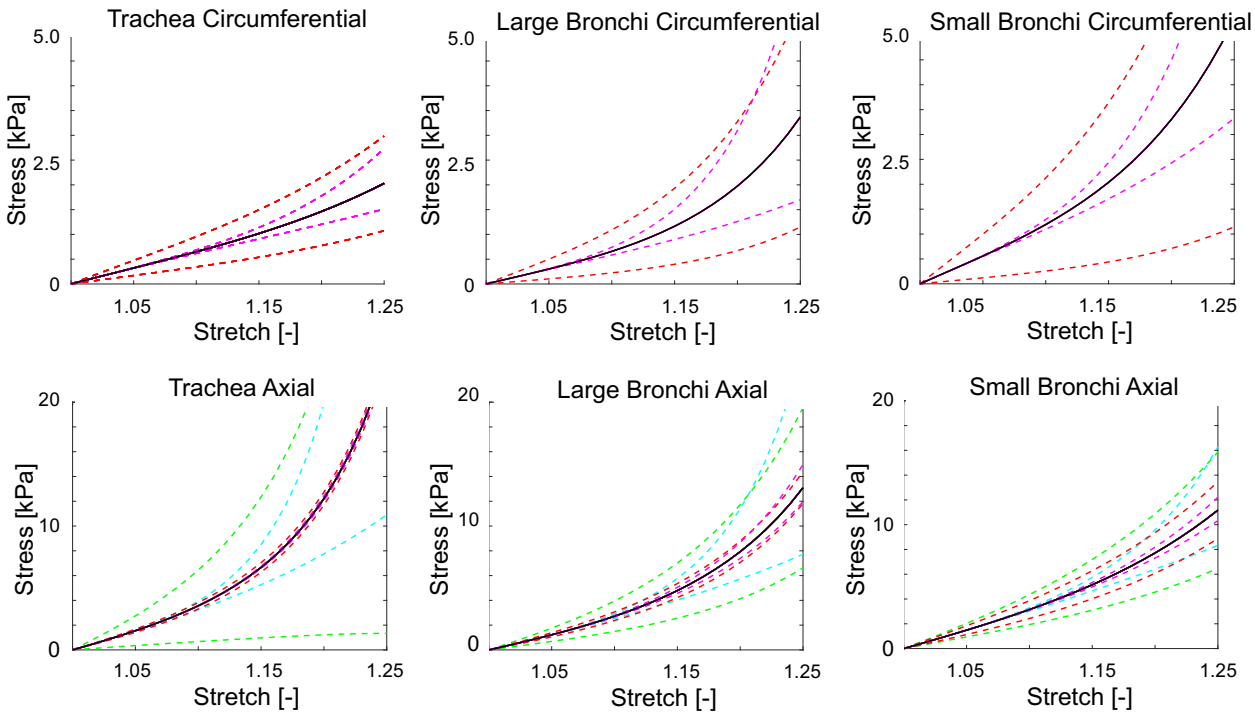

Figure 7: Sensitivity analysis. Top: Incompressible Demiray fit with average (black) μ, β $\pm$standard error of that parameter. Bottom: Combined exponential fiber and IncompressibleDemiray matrix fit with average (black) k_1, k_2, $\pm$ standard error of that parameter. One parameter is varied while others fixed to averages (colored lines).

bronchi (1.67$\pm$ 0.14%) and trachea (0.32$\pm$ 0.51%). The increasing GAG trend from proximal to distal airways generally trends with μ and inversely trends with k_1 and k_2. Collagen content as a percentage of dry weight did not have significant differences between group measurements, however was greatest for small bronchi (17.4$\pm$1.6%) then trachea (14.16$\pm$2.0%) then large bronchi (10.3$\pm$2.8%). Collagen content could be related to β, however the inconclusive correlation to constitutive material properties suggest tissue composition may not be primarily responsible for mechanical function.

3.8. Microstructure Observations

Masson's Trichrome staining of axial slices of unloaded trachea, large bronchi, and small bronchi samples reveal collagen and the elastic fiber system (generically termed and undiscerned between types of collagen or elastic, elaunin, and oxytalan (11)). Regional variation was most notable in the mucosa layer, the nomenclature termed according to Bai et al. (**?**). The fiber system is most visible longitudinally, appearing as dots surrounding the lumen in circumferential images (11; 34; 98; 44). Figure 9 shows connective tissue can be seen in blue and pink, blue staining collagen and pink staining elastin. Evolution of the relative content of collagen to elastin is notable from the trachea to the large bronchi and to the small bronchi. The shape of the fibers remarkably straightens in the small bronchi compared to proximal airways, despite being unloaded samples. The fibers in the trachea have large curvatures: a qualitative increase in wavelength and amplitude is observed compared to distal airways. Tissue architecture heterogeneity is noted when comparing regions of the bronchial network.

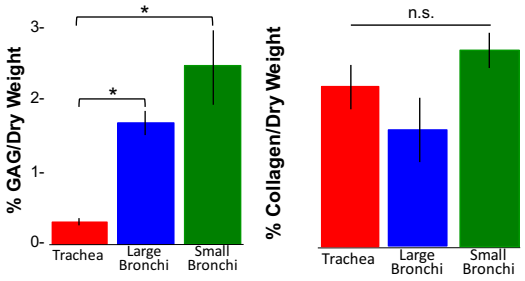

Figure 8: Biochemistry analysis of soft tissue layer (submucosa and mucosa) yielding percentage as a dry weight of glycosaminoglycans (GAG) and collagen content. Significant differences in the GAG content of the trachea to large bronchi and trachea to small bronchi is found. Generally the GAG content increases from proximal to distal regions; this same trend and significant differences was seen for DNA (not shown). Conversely, collagen content was not found to significantly differ between regions, but was noticeably greatest for the small bronchi region (*p<0.05)

4. Discussion

While the model is capable of satisfactorily reproducing exp data, this model is still limited by the form of existing strain-energy functions. Pulmonayr-specific strain energy constitutive formulation based on curvature of stress-streain relation (as with aorta, michael sacks) and other biological tissues can be done. It may be possible that the mechanical paramteres would have direct physical definitions enabling bronchial evolutionary material models, specific to the number generation and the ID of the tissue....where you would be in the model physically is a parameter of its own.

4.1. Mechanical Parameter Correlations

E's relationship with mu and k1....how that changes significance as the stress contribution changes from trachea to large bronchi and small bronchi...

The formulation of the strain-energy function as a matrix and fiber structure provides sufficiently good fit and interactive matrix-fiber behavior not explored.

What does sensitivity tell us? –

Furl of trachea caused by residual stress? No, not seen in human or pig tissue...[cite] Biochemistry – explicit correlations were SURPRISINGLY ..... significance–Gag correlates with what mechanical property. collagen collerates with what? Degrades with disease?

The difference between the mechanics defined by the fiber versus matrix portion of the model for the small bronchi compared to both the trachea and large bronchi is significant. stress contributiuons —-and suggests tissue form may differ enough to impact mechanical function

Histology the elastin goes up in SB — but biochem doesn't show this... The fiber crimp in the trachea suggests loading would first lead to unraveling then bearing of greater loads when taut. While no significant difference in axial stiffness was noted between regions despite the noted fiber curvature in axial images; if fibers are crimped and not solely aligned in the axial direction they would manifest as compliancy compare to straightened fibers as seen in the small bronchi.

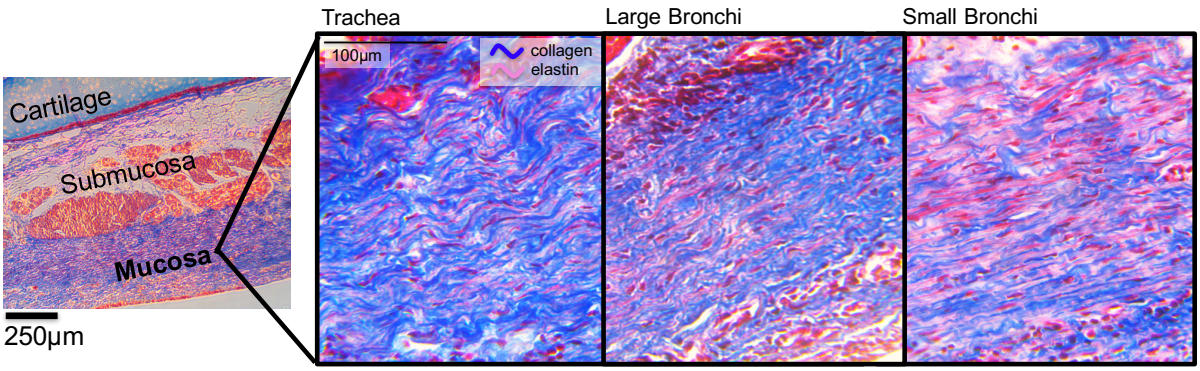

Figure 9: Images of Masson's Trichrome staining. Qualitative comparisons between trachea, large bronchi, and small bronchi observed differences in the mucosa layer. Collagen fibers are blue while elastin fibers in pink. Trachea images have crimped and furled fibers, while small bronchi fiber images appear taut and straightened. A relative increase in elastin fibers are also observed in smaller bronchi in comparison to trachea or large bronchi samples. The altered tissue architecture is suspected to impact mechanical properties.

we do not distinguish beetween elastic fibers (elastin, oxytalic, elaunin)

ALL riregion fits. good fits (high R2) indicate material sufficently captured by fiber+matrox constitutive model— more complex models with dispersed and angled fiber directions can be used in the future, or image-based constitutive modeling Future: Imgae-based constitutive modeling

however, noting the lack of studies exploring these fiber distributions in the bronchial tree (**?**).

tissue is near incompressible....

In order to understand the role of each constitutive law parameter — at zero stretch mu is, k1 is.... beta and k2 are mechanicall what? the urethra paper experimental fit paper

The slope of E-μ is also nearly half that of E-k_1; while the data set were not identical for both graphs shown in Figure 6, this suggests k_1 has greater influence on E than μ.

5. Conclusion

Overall the bronchial tree mechanics is still in its infancy.

We have presented a calibrated lung constitutive model to common constitutive laws. it would be fitting to formulate a model mathematically matching the stress-stretch response particular to lung tissue, as has been done previously for the heart. While the work presented here is necessary, the mathematical response is limited to models meant for polymers and other biological tissues.

Now can we create a anisotropic and heterogenous physiologically respresentative 3D airway model...?

Image based constitutive model the yielding insights to bronchial heterogeneity and providing the will provide the lung mechanics community with computational models the

FEA

Pulmonary medicine needs developments in disease diagnostics, surgical planning, and predictive capabilities seen in parallel biomechanics research on the heart, brain, and muscle.

6. Acknowledgments

This study was supported by the University of California's Provost's Engineering Research Fellowship (PDEF) to Mona Eskandari. We thank the Gladstone Histology and Light Microscopy Core for experimental and technical support for histology.

References

[1] Ambrosi, D.; Ateshian, G.A.; Arruda, E.M.; Cowin, S.C.; Dumais, J; Goriely, A.; Holzapfel, G.A.; Humphrey, J.D.; Kemkemer, R.; Kuhl, E.; Olberding, J.E.; Taber, L.A.; Garikipati, K. Perspectives on biological growth and remodeling. *J Mech Phys Solids.* **2011**, *59*, 863-883.

[2] "Asthma Statistics." Asthma mortality rates have been steadily increasing since the 1970s. **2013**, http:// www.achooallergy.com/asthma- statistics.asp

[3] Amato, M.B.P.; Barbas, C.S.V.; Medeiros, D.M.; Laffey, J.G.; Engelberts, D.; Kavanagh, B. P. Ventilation with lower tidal volumes as compared with traditional tidal volumes for acute lung injury. *N Engl J Med.* **2000**, *343(2000)*, 812-4.

[4] Anafi, R. C.; Wilson, T.A. Airway stability and heterogeneity in the constricted lung. *J Appl Phys.* **2001**, *91(3)*, 1185-1192.

[5] Avazmohammadi, R., Hill, M. R., Simon, M. A., Zhang, W., Sacks, M. S. (2017). A novel constitutive model for passive right ventricular myocardium: evidence for myofiber-collagen fiber mechanical coupling. Biomechanics and modeling in mechanobiology, 16(2), 561-581.

[6] Bai, T.R.; Knight, D.A. Structural changes in the airways in asthma: observations and consequences. *Clinical Science.* **2005**, *108*, 463-477.

[7] Bai, A.; Eidel, D.H.; Hogg, J.C.; James, A.L.; Lambert, R.K.; Ludwig, M.S.; Martin, M.; McDonald, D.M.; Mitzner, W.A.; Okazawa, M.; Pack, R.J.; Paré,P.D.; Schellenberg, R.R.; Tiddens, H.A.; Wagner, E.M.; Yager, D. Proposed nomenclature for quantifying subdivisions of the bronchial wall. *J Appl Phys.* **1994**, *77*, 1011-1014.

[8] Barnett S.B.; Nurmagambetov T.A.; Costs of asthma in the United States: 2002-2007. *J Allergy Clin Immunol.* **2011**, *127*, 145-152.

[9] Blaber, J.; B. Adair; Antoniou A. Ncorr: open-source 2D digital image correlation matlab software. *Exp Mech.* **2015**, *55.6*, 1105-1122.

[10] Black, P. N., Ching, P. S., Beaumont, B., Ranasinghe, S., Taylor, G., Merrilees, M. J. (2008). Changes in elastic fibres in the small airways and alveoli in COPD. European Respiratory Journal.

[11] Bock, P., Stockinger, L. (1984). Light and electron microscopic identification of elastic, elaunin and oxytalan fibers in human tracheal and bronchial mucosa. Anatomy and embryology, 170(2), 145-153.

[12] Brackel, H.J.; Pedersen, O.F.; Mulder, P.G.; Overbeek, S.E.; Kerrebijn, K.F.; Bogaard, J. M. Central airways behave more stiffly during forced expiration in patients with asthma. *Am J Respir Crit Care Med.* **2000**, *162*, 896-904.

[13] Budday, S.; Nay, R.; de Rooij, R.; Steinmann, P.; Wyrobek, T.; Ovaert, T. C.; Kuhl, E. Mechanical properties of gray and white matter brain tissue by indentation. *J Mech Behav Biomed Mat.* **2015**, *46*, 318-330.

[14] Butler, B. J.; Williams, A.; Tucker, A. W.; Proud, W. G.; Brown, K. A. Comparative quasi-static mechanical characterization of fresh and stored porcine trachea specimens. *Euro Phys S Special Top* **2018**, *227(1-2)*, 55-60.

[15] Carniel, T. A., Fancello, E. A. (2017). A transversely isotropic coupled hyperelastic model for the mechanical behavior of tendons. Journal of biomechanics, 54, 49-57.

[16] Codd, S.L.; Lambert, R.K.; Alley, M.R.; Pack, R.J. Tensile stiffness of ovine tracheal wall. *J Appl Phys.* **1994**, *76*, 2627-2635.
[17] Cosio, M., Ghezzo, H., Hogg, J. C., Corbin, R., Loveland, M., Dosman, J., Macklem, P. T. (1978). The relations between structural changes in small airways and pulmonary-function tests. New England Journal of Medicine, 298(23), 1277-1281.
[18] Devore, J. L. (1991). Probability and Statistics for Engineering and The Sciences, Duxbury Press, Belmont, CA.
[19] Ernst, A.; Herth, F.J.F. (Eds). Principles and practice of interventional pulmonology. *Springer Science & Business Media.* **2012**.
[20] Eskandari M.; Pfaller M.R.; Kuhl E. On the role of mechanics in chronic lung disease. *Materials.* **2013**, *6*, 5639-5658.
[21] Eskandari, M; Kuschner, W.G; Kuhl, E. Patient-specific airway wall remodeling in chronic lung disease. *Ann Biomed Eng.* **2015**, *10*, 2538-2551.
[22] Eskandari, M; Kuhl, E. Systems biology and mechanics of growth. *WIREs Syst Biol Med.* **2015**, *7*, 401-412.
[23] Eskandari, M; Javili, A; Kuhl, E. Elastosis during airway wall remodeling explains multiple coexisting instability patterns. *J Theor Bio.* **2016**, *403*, 209-218.
[24] Eskandari, M., Arvayo, A.L., Levenston, M.E. (2018) Mechanical Properties of the Airway Tree: Heterogeneous and Anisotropic Pseudoelastic and Viscoelastic Tissue Responses. Journal of applied physiology.
[25] Dey, P. Basic and Advanced Laboratory Techniques in Histopathology and Cytology.
[26] Fung YC. Biomechanics: Mechanical Properties of Living Tissue. *New York: Springer-Verlag*, **1993**.
[27] "Gold Reports 2017." Global Initiative for Chronic Obstructive Lung Disease - GOLD, **2017**, goldcopd.org/gold-reports-2017/
[28] Gillis, H.L.; Lutchen, K.R. Airway remodeling in asthma amplifies heterogeneities in smooth muscle shortening causing hyperresponsiveness. *J Appl Phys*, **1999** *86(6)*, 2001-2012.
[29] Gross, N. J. The GOLD standard for chronic obstructive pulmonary disease. *Am J Res Crit Care Med.* **2001**, *163(5)*, 1047-1048.
[30] Gunst, S.J.; Stropp, J.Q. Pressure-volume and length-stress relationships in canine bronchi in vitro. *J Appl Phys.* **1988**, *64(6)*, 2522-2531.
[31] Guo, X.; Kassab, G.S. Variation of mechanical properties along the length of the aorta in C57bl/6 mice. *Am J Phys-Heart & Circ Phys.* **2003**, *285(6)*, H2614-H2622.
[32] Guerin, H. A., Elliott, D. M. (2005). The role of fiber-matrix interactions in a nonlinear fiber-reinforced strain energy model of tendon. Journal of biomechanical engineering, 127(2), 345-350.
[33] Hoffman, B.; Martin, M.; Brown, B. N.; Bonassar, L. J.; Cheetham, J. Biomechanical and biochemical characterization of porcine tracheal cartilage. *The Laryngoscope* **2016**, *126(10), E325-E331.*
[34] Hogg, J.C.; Chu, F.; Utokaparch, S.; Woods, R.; Elliott, W.M.; Buzatu, L.; Cherniack, R.M.; Rogers, R.M.; Sciurba, F.C.; Coxson, H.O.; Pare, P.D. The nature of small-airway obstruction in chronic obstructive pulmonary disease. New Engl J Med. **2004**, 350*, 2645-2653.*
[35] Holzapfel, G. A. Biomechanics of soft tissue. The handbook of materials behavior models, **2001**, 3(1)*, 1049-1063.*
[36] Holzapfel, G. A., Ogden, R. W. (2009). Constitutive modelling of passive myocardium: a structurally based framework for material characterization. Philosophical Transactions of the Royal Society of London A: Mathematical, Physical and Engineering Sciences, 367(1902), 3445-3475.
[37] Holzapfel, G. A.; Ogden, R. W. Comparison of two model frameworks for fiber dispersion in the elasticity of soft biological tissues. Euro J Mech-A/Solids. **2017**, 66*, 193-200.*
[38] Hoppin, F.G.; Hughes, J.M.; Mead, J.E.R.E. Axial forces in the bronchial tree. J Appl Phys. **1977**, 42(5)*, 773-781.*
[39] Hrousis, C.A.; Wiggs B.R.; Drazen J.M.; Parks D.M.; Kamm R.D.; Mucosal Folding in Biologic Vessels. Journal of Biomech Eng. **2002**, 124*, 334-341.*
[40] Humphrey, J. D., Yin, F. C. P. (1987). On constitutive relations and finite deformations of passive

cardiac tissue: I. A pseudostrain-energy function. Journal of biomechanical engineering, 109(4), 298-304.

[41] Hurtado, D. E., Villarroel, N., Andrade, C., Retamal, J., Bugedo, G., Bruhn, A. (2017). Spatial patterns and frequency distributions of regional deformation in the healthy human lung. Biomechanics and modeling in mechanobiology, 16(4), 1413-1423.

[42] James, A.L.; Paré, P.D.; Hogg, J.C.; The mechanics of airway narrowing in asthma. Am Rev Respir Disease. **1989***,* 139*, 242-246.*

[43] Jeffery, P. K. (2001). Remodeling in asthma and chronic obstructive lung disease. American journal of respiratory and critical care medicine, 164(supplement_2), S28-S38.

[44] Kamel, K. S.; Beckert, L. E.; Stringer, M. D. Novel insights into the elastic and muscular components of the human trachea. Clinical Anatomy **2009***,* 22(6)*, 689-697.*

[45] Kamm, R.D. Airway wall mechanics. *Ann Rev Biomed Eng.* **1999**, *1*, 47-72.

[46] Khan, M. A.; Ellis, R.; Inman, M. D.; Bates, J. H.; Sanderson, M. J.; Janssen, L. J. Influence of airway wall stiffness and parenchymal tethering on the dynamics of bronchoconstriction. *Am J Phys-Lung Cell & Mol Phys.* **2010**, *299(1)*, L98-L108.

[47] Knight, D.A. (2005). Structural changes in the airways in asthma: observations and consequences. Clinical science, 108(6), 463-477.

[48] Kuwano, K., Bosken, C. H., Pare, P. D., Bai, T. R., Wiggs, B. R., Hogg, J. C. (1993). Small airways dimensions in asthma and in chronic obstructive pulmonary disease. The American review of respiratory disease, 148(5), 1220.

[49] Lambert, R. K.; Wilson, T. A.; Hyatt, R. E.; Rodarte, J. R. A computational model for expiratory flow. *J Appl Phys.* **1982** em 52(1), 44-56.

[50] Lambert, R.K. Role of bronchial basement membrane in airway collapse. *J Appl Phys.* **1991**, *71*, 666-673.

[51] Lambert, R. K.; Pare, P. D.; Okazawa, M. Stiffness of peripheral airway folding membrane in rabbits. *J Appl Phys.* **2001**, *90(6)*, 2041-2047.

[52] Leslie, K.O.; Wick M. Practical Pulmonary Pathology E-Book: A Diagnostic Approach. *Elsevier Health Sciences* **2011**.

[53] Lutchen, K. R., Pare, P. D., Seow, C. Y. (2017). Hyperresponsiveness: relating the intact airway to the whole lung. Physiology, 32(4), 322-331.

[54] Mead-Hunter, R., King, A. J., Larcombe, A. N., Mullins, B. J. (2013). The influence of moving walls on respiratory aerosol deposition modelling. Journal of Aerosol Science, 64, 48-59.

[55] Masri, C., Chagnon, G., Favier, D., Sartelet, H., Girard, E. (2018). Experimental characterization and constitutive modeling of the biomechanical behavior of male human urethral tissues validated by histological observations. Biomechanics and modeling in mechanobiology, 1-12.

[56] Mauad, T.; Xavier, A. Elastosis and fragmentation of fibers of the elastic system in fatal asthma. *Am J Respir Crit Care Med.* **1999**, *160*, 968-975.

[57] Moulton, D.E.; Goriely, A. Possible role of differential growth in airway wall remodeling in asthma. *J Appl Physiol.* **2011**, *110*, 1003-1012.

[58] McFawn, P.K.; Mitchell, H.W. Bronchial compliance and wall structure during development of the immature human and pig lung. *Euro Resp J.* **1997**, *10.1*, 27-34.

[59] McKay, K.O.; Wiggs, B.R.; Pare, P. D.; Kamm, R.D. Zero-stress state of intra-and extraparenchymal airways from human, pig, rabbit, and sheep lung. *J Appl Phys.* **2002**, *92(3)*, 1261-1266.

[60] *Chronic Obstructive Pulmonary Disease (COPD).* Centers for Disease Control and Prevention. **4 Aug. 2017**, *www.cdc.gov/copd/index.html*#2.

[61] Noble, P. B., Turner, D. J., Mitchell, H. W. (2002). Relationship of airway narrowing, compliance, and cartilage in isolated bronchial segments. Journal of Applied Physiology, 92(3), 1119-1124.

[62] Noble, P.B.; Sharma, A.; McFawn, P.K.; Mitchell, H.W. Airway narrowing in porcine bronchi with and without lung parenchyma. *Euro Resp J.* **2005**, *26(5)*, 804-811.

[63] Noble, P.B.; Sharma, A.; McFawn, P.K.; Mitchell, H.W. Elastic properties of the bronchial mucosa: epithelial unfolding and stretch in response to airway inflation. *J Appl Phys.* **2005**, *99(6)*, 2061-2066.

[64] Noble, P.B.; McLaughlin, R.A.; West, A.R.; Becker, S.; Armstrong, J.J.; McFawn, P. K.; Eastwood, P.; Hillman, D.R.; Sampson, D.; Mitchell, H.W. Distribution of airway narrowing responses across generations and at branching points, assessed in vitro by anatomical optical coherence tomography. *Resp Research* **2010**, *11(1)*, 9.

[65] Noble, P. B.; Hernandez, J. M.; Mitchell, H. W.; Janssen, L. J. Deep inspiration and airway physiology: human, canine, porcine, or bovine? *J Appl Phys.* **2010**, *109(3)*, 938-939.

[66] Oakes, J. M.; Shadden, S. C.; Grandmont, C.; Vignon?Clementel, I. E. Aerosol Transport Throughout Inspiration and Expiration in the Pulmonary Airways. *Int J Num Meth Biomed Eng.* **2016**.

[67] O'Connell, G. D., Guerin, H. L., Elliott, D. M. (2009). Theoretical and uniaxial experimental evaluation of human annulus fibrosus degeneration. Journal of biomechanical engineering, 131(11), 111007.

[68] O'Connell, G. D. (2009). Degeneration affects the structural and tissue mechanics of the intervertebral disc.

[69] Okazawa, M.; D?Yachkova, Y.; Pare, P.D. Mechanical properties of lung parenchyma during bronchoconstriction. *J Appl Phys.* **1999**, *86(2)*, 496-502.

[70] Otis Jr, D. R.; Ingenito, E. P.; Kamm, R. D.; Johnson, M. Dynamic surface tension of surfactant TA: experiments and theory. *J Appl Phys.* **1994**, *77(6)*, 2681-2688.

[71] Peng, X., Madany, A.M., Jang, J.C., Valdez, J.M., Rivas, Z., Burr, A.C., Grinberg, Y.Y., Nordgren, T.M., Nair, M.G., Cocker, D. and Carson, M.J., 2018. Continuous Inhalation Exposure to Fungal Allergen Particulates Induces Lung Inflammation While Reducing Innate Immune Molecule Expression in the Brainstem. ASN neuro, 10, p.1759091418782304.

[72] Perlman, C. E., Bhattacharya, J. (2007). Alveolar expansion imaged by optical sectioning microscopy. Journal of applied physiology, 103(3), 1037-1044.

[73] Politi, A. Z.; Donovan, G. M.; Tawhai, M. H.; Sanderson, M. J.; Lauzon, A. M.; Bates, J. H.; Sneyd, J. A multiscale, spatially distributed model of asthmatic airway hyper-responsiveness. *J Theo Bio.* **2010**, *2664* 614-624.

[74] Quanjer, P. H., Tammeling, G. J., Cotes, J. E., Pedersen, O. F., Peslin, R., Yernault, J. (1993). Lung volumes and forced ventilatory flows.

[75] Ratnovsky, A.; Regev, N.; Wald, S.; Kramer, M.; Naftali, S. Mechanical properties of different airway stents. *Med Engr & Phys.* **2015**, *37(4)*, 408-415.

[76] Rattue, Petra. "Lung Diseases Leading Cause Of Death, Most People Don't Know." *Medical News Today*, MediLexicon International. **1 July 2012**, *www.medicalnewstoday.com/articles/*247293*.php.*

[77] Razavi, M. J.; Pidaparti, R.; Wang, X. Surface and interfacial creases in a bilayer tubular soft tissue. *Phys Rev E.* **2016**, *94*, 022405.

[78] Reddel, C. J., Weiss, A. S., Burgess, J. K. (2012). Elastin in asthma. Pulmonary pharmacology and therapeutics, 25(2), 144-153.

[79] Roberts, C.R.; Rains, J.K.; Pare, P.D.; Walker, D.C.; Wiggs, B.; Bert, J.L. Ultrastructure and tensile properties of human tracheal cartilage. *J Biomec.* **1997**, *31* 81–86.

[80] Robertson, C.; Lee, S.W.; Ahn, Y.C.; Mahon, S.; Chen, Z.; Brenner, M.; George, S.C. Investigating in vivo airway wall mechanics during tidal breathing with optical coherence tomography. *J Biomed Opt.* **2011**, *16(10)*, 106011-106011.

[81] Sacks, M. S. (2000). Biaxial mechanical evaluation of planar biological materials. Journal of elasticity and the physical science of solids, 61(1-3), 199.

[82] Safshekan, F., Tafazzoli-Shadpour, M., Abdouss, M., Shadmehr, M. B. (2016). Mechanical characterization and constitutive modeling of human trachea: age and gender dependency. Materials, 9(6), 456.

Safshekan, F.; Tafazzoli-Shadpour, M.; Abdouss, M.; Shadmehr, M. B. Viscoelastic properties of human tracheal tissues. *J Biomech Engr.* **2017**, *139(1)*, 011007.

[83] Seow, C. Y., Wang, L., Pare, P. D. (2000). Airway narrowing and internal structural constraints. Journal of Applied Physiology, 88(2), 527-533.

[84] Seyfi, B.; Santhanam, A.P.; Ilegbusi, O.J. A Biomechanical Model of Human Lung Deformation Utilizing Patient-Specific Elastic Property. *J Cancer Ther.* **2016**, *7(06)*, 402.

[85] Sinclair, S.E.; Molthen, R.C.; Haworth, S.T.; Dawson, C.A.; Waters, C.M. Airway strain during mechanical ventilation in an intact animal model. *Am J Resp Crit Care Med*, **2007**, *176(8)*, 786-794.
[86] Suki, B.; Bates, J. H. Lung tissue mechanics as an emergent phenomenon. *J Appl Phys.* **2011** *110(4)*, 1111-1118.
[87] Spencer, A. J. M. (1984). Constitutive theory for strongly anisotropic solids. In Continuum theory of the mechanics of fibre-reinforced composites (pp. 1-32). Springer, Vienna.
[88] Teng, Z.; Ochoa, I.; Li, Z.; Lin, Y.; Rodriguez, J. F.; Bea, J. A.; Doblare, M. Nonlinear mechanical property of tracheal cartilage: A theoretical and experimental study. *J Biomech.* **2008**, *41(9)*, 1995-2002.
[89] Teng, Z.; Trabelsi, O.; Ochoa, I.; He, J.; Gillard, J.H.; Doblare, M. Anisotropic material behaviours of soft tissues in human trachea: an experimental study. *J Biomech.* **2012**, *45(9)*, 1717-1723.
[90] Terry, B.S.; Wang, X.; Schoen, J.A.; Rentschler, M.E. A preconditioning protocol and biaxial mechanical measurement of the small intestine. *Int J Exp Comp Biomech.* **2014**, *2(4)*, 293-309.
[91] Trabelsi, O., Del Palomar, A. P., Lopez-Villalobos, J. L., Ginel, A., Doblare, M. (2010). Experimental characterization and constitutive modeling of the mechanical behavior of the human trachea. Medical engineering and physics, 32(1), 76-82.
[92] Vawter, D. L., Fung, Y. C., West, J. B. (1979). Constitutive equation of lung tissue elasticity. Journal of Biomechanical Engineering, 101(1), 38-45.
[93] Virchow, J. C. Asthma–a small airway disease: concepts and evidence. *Pneumologie* (Stuttgart, Germany), **2009**, *63* S96-101.
[94] Wall, W. A., Rabczuk, T. (2008). Fluid–structure interaction in lower airways of CT-based lung geometries. International Journal for Numerical Methods in Fluids, 57(5), 653-675.
[95] Wang, L.; Tepper, R.; Bert, J.L.; Pinder, K. L.; Pare, P. D.; Okazawa, M. Mechanical properties of the tracheal mucosal membrane in the rabbit. I. Steady-state stiffness as a function of age. *J Appl Phys.* **(2000)**, *88(3)*, 1014-1021.
[96] Wang, L.; Pinder, K. L.; Bert, J. L.; Okazawa, M.; Pare, P. D. Mechanical properties of the tracheal mucosal membrane in the rabbit. II. Morphometric analysis. *J Appl Phys.* **(2000)**, *88(3)*, 1022-1028.
[97] Weibel E.R. Morphometry of the Human Lung. New York: Academic Press, 1963, p. 139.
[98] Wiggs, B.R.; Hrousis, C.A.; Drazen, J.M.; Kamm, R.D. On the mechanism of mucosal folding in normal and asthmatic airways. *J Appl Phys.* **1997**, *83*, 1814-1821.
[99] Wiechert, L.; Comerford, A.; Rausch, S.; Wall, W. Advanced multi-scale modelling of the respiratory system. *Fund Med & Eng Inv Protect Artif Resp.* **2011**, *116*, 1-32.
[100] Wilson, L.; Devine, E. B.; So, K. Direct medical costs of chronic obstructive pulmonary disease: chronic bronchitis and emphysema. *Respir Med.* **2000**, *83*, 204-213.
[101] Yang, L., Li, J., Mo, H., Pidaparti, R. M., Witten, T. M. Possible role of collagen reorientation during airway remodeling on mucosal folding. *J Engr Math.* **2015**.
[102] Yin, Y., Choi, J., Hoffman, E. A., Tawhai, M. H., Lin, C. L. (2010). Simulation of pulmonary air flow with a subject-specific boundary condition. Journal of biomechanics, 43(11), 2159-2163.
[103] Yoshihara, L., Ismail, M., Wall, W. A. (2013). Bridging scales in respiratory mechanics. In Computer Models in Biomechanics (pp. 395-407). Springer, Dordrecht.
[104] Xi, J., Longest, P. W. (2007). Transport and deposition of micro-aerosols in realistic and simplified models of the oral airway. Annals of biomedical engineering, 35(4), 560-581.
[105] Zhao, L.; Sundaram, S.; Le, A.V.; Huang, A.H.; Zhang, J.; Hatachi, G.; Beloiartsev, A.; Caty, M.G.; Yi, T.; Leiby, K.; Gard, A. Engineered Tissue Stent Biocomposites as Tracheal Replacements. *Tissue Eng Part A.* **2016**, *22(17-18)*, 1086-1097.